Hindawi
Advances in Materials Science and Engineering
Volume 2019, Article ID 5234327, 17 pages
https://doi.org/10.1155/2019/5234327

Research Article

Mesoscopic Numerical Simulation of Fracture Process and Failure Mechanism of Concrete Based on Convex Aggregate Model

Yijiang Peng, Xiyun Chen, Liping Ying, Ying Chen, and Lijuan Zhang

Key Laboratory of Urban Security and Disaster Engineering, Ministry of Education, Beijing University of Technology, Beijing 100124, China

Correspondence should be addressed to Liping Ying; 717519705@qq.com

Received 12 August 2018; Accepted 25 December 2018; Published 22 January 2019

Academic Editor: Aniello Riccio

To investigate the fracture process and failure mechanism of concrete subjected to uniaxial compressive loading, a new finite element method—the base force element method (BFEM)—was adopted in the modeling of numerical simulation. At mesoscale, concrete is considered as a three-phase heterogeneous material composed of aggregate particles, cement mortar, and the interfacial transition zones between the two phases. A two-dimensional random convex aggregate model was established using the principle of the area equivalence method. A multistage linear damage constitutive model that can describe nonlinear behavior of concrete under mechanical stress was proposed. The mechanical properties of concrete mesoscopic components are determined. The numerical simulation results indicate that the base force element method can be applied to predict the failure pattern of concrete under compressive loading, which have a good accordance with the available experiment data. The stress contour plots were given and used to analyze the failure mechanism of concrete. The effects of specimen size on the strength of concrete material were studied. It is found that compressive strength of concrete decreases as the specimen size increases. In addition, the influences of aggregate distribution, coarse aggregate content, and end friction on concrete performance are explored.

1. Introduction

The usage of the concrete is increasing with the development of modern civil engineering. As the most widely used construction materials, the researches on the macromechanical properties and the strength for concrete materials of concrete material has important theoretical significance for the reliability in designing concrete structures, especially for the complex structures. It is found that the failure behavior of concrete is complex even under normal loading conditions. In macrolevel, it is hard and incomprehensive to describe the mechanical properties and failure mechanism of concrete material due to the limitations of the laboratory experiment, time-consumption, and environmental factors of the test.

Wittmann et al. [1] Schlangen and van Mier [2] are those of the early scholars to study the mechanical properties of concrete from the microscopic level using numerical analysis methods. The use of numerical analysis methods to study concrete is also known as "numerical concrete." Until now, advanced mesoscopic mechanics analysis theory and computer technology efforts contribute to explore the numerical simulation of damage process and the influence on material damage in concrete with the finite element method. In mesoscopic structure, concrete is a complex heterogeneous composite material, whose fracture pattern and the macroscopic mechanical nonlinear behavior can be attributed to the properties and mix proportion of internal mesoscopic composition, such as aggregate particles distribution, aggregate particles size, aggregate particles shape, cement mortar properties, interfacial properties, and microcrack [3]. That is to say, the obviously random characteristics of macroscopic mechanical properties were reflected entirely by the global strength and stress-strain full curve which are mainly caused by its internal mesoscopic heterogeneity and randomness of concrete materials.

There is an obvious size effect phenomenon that the larger dimension structures more likely fail at relatively smaller loading. This phenomenon in quasi-brittle structures is related to a transition from ductile behavior of small specimens to a totally brittle response of large ones [4, 5].

Also, the study of size effect has been observed in [6–8]. The behavior of size effect has been widely accepted which is contributed by the effect of internal materials, and some were based on the principles of fracture mechanics [9–11]. Fracture mechanics was first employed in the study of fracture mechanism in concrete materials [12], and a large amount of classical cracking models was established, such as two parameter fracture model [13], virtual fracture model [14], and equivalent fracture model. Nevertheless, without take into account the existence of microcracks that is the main reason for formation and propagation of cracks and also eventual failure of concrete [9, 15], the mechanical properties and fracture mechanism of concrete was difficult to reasonably predict using fracture mechanics theory.

Therefore, the microscopic damage mechanics theory was proposed to make up the limitation of the fracture mechanics concept which neglected the process before macrocracks appeared (i.e., microcracks and microdefects). Accordingly, numerous researches have focused on simulating the damage process of concrete considering its mesoscopic composition characteristics. Typically, the lattice model [16], the micromechanical model [17], the random aggregate model [18], and the mesoelement equivalent model [19]. Varieties of numerical models of mesoscopic mechanics were developed from two dimension to three dimension which made significant progress in ensuring the accuracy of numerical simulation [20, 21].

The concept of damage variable was proposed because of the rise of damage mechanics theory and was combined with continuum mechanics in the effort of [22] to describe the continuous change of material damage, especially the strain softening characteristic. As one of the essential issues of continuous damage mechanics, the damage constitutive relation of material has been studied, which includes elastic damage, plastic damage, and elastoplastic damage. In the previous work, concrete is the quasi-brittle material that had no obvious irreversible deformation after external stress. The investigations [23–25] have indicated that the failure behavior of concrete subjected to uniaxial loading was able to be described by the elastic damage constitutive model considering the influence of damage on stiffness because of the brittle characteristics.

So far, the technology of concrete aggregate placement is the most concerned in numerical simulation on the mesostructure. In order to simplify the calculation, a single aggregate model was proposed [26] to analyze the damage of concrete under uniaxial compression loading. It was found that aggregate-mortar interface is the weakest link and main reason of inelasticity. Buyukozturk [27] developed the nine circular aggregates model to study the strength and failure mechanism of concrete with the loadings of uniaxial and biaxial compressions. Considering the influence of aggregate distribution on the complex performance of concrete, several efforts have been made in consistent with the actual concrete in the statistical sense. Bazant et al. [28] used the random circle particle model that can describe realistically the localization and propagation of cracks which agreed with experiments. In addition, they [29, 30] had published a number of papers in recent years on comparisons between Bazant size effect model (SEM) and Hu-Duan boundary effect model (BEM) for quasi-brittle fracture of concrete. Hu et al. [31, 32] introduced the maximum aggregate size into BEM, established the corresponding prediction equations, and analyzed and compared the essential difference and application function of SEM and BEM. Based on this, they explained the internal mechanism of structural damage size effect.

However, few researches have focused on that the aggregate shape may also affect the properties of concrete. Wittmann et al. [1] presented the random distributed geometry of the natural aggregates model including round and polygon to investigate the effective properties, e.g., the diffusion coefficient and the modulus of elasticity of concrete material. The methods for generating polygon or polyhedron aggregate can be concluded as two types: one was generated new vertices and surfaces from the surroundings of a convex matrix until the requirement was satisfied [18, 33, 34] and the other was using a Delaunay triangulation which divided the available space into separate areas.

In recent years, a new type of finite element method, the base force element method (BFEM), has been developed by Peng and Liu [37] based on the concept of the base forces by Gao [38]. This method takes the base force vector (first-order tensor) as an unknown basic quantity, and it has many advantages. For example, it has concise and integral explicit finite element formulation without numerical integration. Moreover, the programming is simple, and the calculation accuracy is high. Furthermore, the base force element method (BFEM) on potential energy principle was used to analyze recycled aggregate concrete on mesoscale [39].

In this paper, the base force element method (BFEM) is applied to investigate the failure pattern of common concrete with polygon aggregate subjected to uniaxial compressive loading in two dimensions. In mesostructure, concrete is assumed as a three-phase composite material taking its heterogeneous into account. To generate random convex polygonal aggregates on the basis of circle aggregates, correspondingly, according to the Monte Carlo principle, the mechanical properties of mesostructure for concrete were assumed to obey the Weibull distribution. An elastic damage constitutive model is adopted with the nonlinear behavior analysis of concrete material. The good relation with available test data confirms the accuracy and feasibility of the present mesoscopic simulation approach. A series of concrete specimens with different sizes, different aggregate distributions, different aggregate contents, and different end frictions are designed to analyze failure mechanism and the mechanical behavior of concrete from mesolevel.

2. Theory of Base Force Element

The concept of base forces was proposed by Gao [38]. The base forces are used to replace various stress tensors for the description of the stress state at a point. These base forces can be directly obtained from the strain energy. By means of the base forces, the equilibrium equation, boundary condition, and elastic law are written in very simple forms. For large

deformation problems, the derivation of basic formulae was simplified.

The base force element method (BFEM) on complementary energy principle uses the base forces as fundamental variables to establish control equations of the novel finite element method. In the literature [38], Gao gave an new idea of deriving compliance matrix of an arbitrary polyhedron element. Peng and Liu [37] gave an explicit expression of the compliance matrix and derived governing equations of the BFEM on complimentary energy principle using the Lagrange multiplier method. The new finite element method based on the concept of base forces was called as the base force element method by Peng and Liu [37].

The BFEM on potential energy principle uses the displacement gradients $\mathbf{u}_i$ which are the conjugate variables of base forces $\mathbf{T}^i$ to establish control equations of the new finite element method. Peng and Liu [37] derived governing equations of the BFEM on potential energy principle using Gao's thought for a triangular element as shown in Figure 1. The stiffness matrix of a base force element [39] can be obtained as

$$\mathbf{K}^{IJ} = \frac{E}{2A(1+\nu)}\left[\frac{2\nu}{1-2\nu}\mathbf{m}^I \otimes \mathbf{m}^J + \mathbf{m}^{IJ}\mathbf{U} + \mathbf{m}^J \otimes \mathbf{m}^I\right], \quad (I = 1,2,3, J = 1,2,3), \tag{1}$$

where E is Young's modulus of an element, ν is Poisson's ratio, A is the area of the element, $\mathbf{U}$ is the unit tensor, expressed as $\mathbf{U} = \mathbf{P}_\alpha \otimes \mathbf{P}^\alpha = \mathbf{P}^\alpha \otimes \mathbf{P}_\alpha$, and $\mathbf{m}^{IJ} = \mathbf{m}^I \cdot \mathbf{m}^J$, and $\mathbf{m}^I$ can be calculated from

$$\mathbf{m}^I = \mathbf{m}^I_\alpha \mathbf{P}_\alpha = \frac{1}{2}\left(L_{IJ}\mathbf{n}^{IJ} + L_{IK}\mathbf{n}^{IK}\right), \tag{2}$$

where $\mathbf{P}_\alpha$ is the basic vector and $\mathbf{P}^\alpha$ is the conjugate vector of $\mathbf{P}_\alpha$; L_{IJ} and L_{IK} are the length of edges IJ and IK of the element; and $\mathbf{n}^{IJ}$ and $\mathbf{n}^{IK}$ denote the external normal of edges IJ and IK, respectively.

For the plane stress problem, it is necessary to replace $E/(1-\nu^2)$ by E and $\nu/(1-\nu)$ by ν in equation (1).

3. Convex Polygon Aggregate

Concrete is an inhomogeneous composite material that the macroperformance is strongly related to its mesocomposition. Generally speaking, concrete was regarded as a three-phase composite material consisting of coarse aggregates, cement mortar, and the interface transition zones (ITZs) between aggregates and cement mortar at mesolevel. As known, internal structural characteristics will change causing the different properties of concrete when applied loading. As the main reason of this change, its internal material heterogeneity has the influence on damage behavior of concrete. Therefore, the aggregate shapes should be noted to ensure that the characteristic of mesostructure material is accurately represented.

The aggregate type of concrete determines the shape of aggregate particles, generally speaking, including two types; gravel aggregates have a round shape, while crushed rock aggregates has an angular shape [18, 19]. A convex polygon aggregate model was created in this paper to simulate real aggregates. The concrete material containing convex aggregate is considered to have three-phase media, as shown in Figure 2. Compared with the work of [39], the effect of aggregate type is explored.

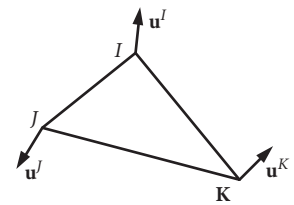

Figure 1: A triangular element.

3.1. Polygon-Based Framework. The method is to generate particles with a randomly shaped polygon-based framework which is divided into triangles, quadrilaterals, and pentagons according to the classification of aggregate size on the boundary of the round coarse aggregates at first. The adjacent vertexes of the polygon-based framework are controlled by the following equation:

$$L_{\min} = 2R \cdot \sin\left(\frac{\pi}{2(n-1)}\right), \tag{3}$$

where $L_{\min}$ is the minimum distance between adjacent vertexes of the base frame. R is the radius of the aggregate. n is the number of vertexes in the polygon-based framework. The area of the newly generated convex aggregate must reach the original aggregate area. The new convex polygon aggregate is illustrated in Figure 3.

3.2. Convex Polygon Generation. In Figure 4, the vertices of any convex polygon can be ordered in counterclockwise as $A_1, A_2, A_3, \ldots, A_i, A_{i+1}, \ldots, A_n$; correspondingly, the coordinates are $(x_1, y_1), (x_2, y_2), (x_3, y_3), \ldots, (x_i, y_i), (x_{i+1}, y_{i+1}), \ldots, (x_n, y_n)$. A new vertex in the outer semicircle is inserted so that the diameter is the longer side of the polygon. In order to improve the generation efficiency of the convex polygons, the slope of the longest side and the angle β of the X-axis should be first calculated, as shown in Figure 4. Therefore, the coordinates of the new insertion point P can be evaluated by equation (4) [18] in the following forms:

$$\begin{cases} x_p = \dfrac{1}{2}\left(x_i + x_{i+1}\right) + \dfrac{1}{2}\overline{A_i + A_{i+1}}R_1\cos\left(2\pi R_2\right), \\ y_p = \dfrac{1}{2}\left(y_i + y_{i+1}\right) + \dfrac{1}{2}\overline{A_i + A_{i+1}}R_1\cos\left(2\pi R_2\right), \end{cases} \tag{4}$$

where R_1 and R_2 are, respectively, the random numbers from 0 to 1. Herein, the new insertion point P cannot exceed the scope of the specimen, namely, x_p and y_p that ranges between 0 to b and 0 to h, where b and h are the width and height of the specimen, respectively.

After the new vertex of the polygon is obtained, it is necessary to determine whether the two new edges, PA_i

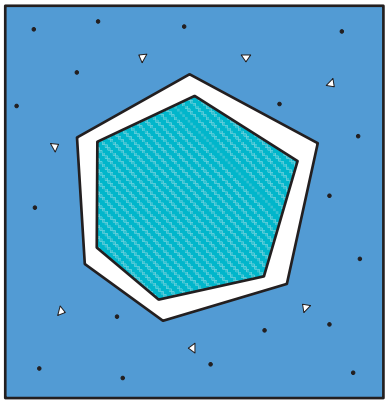

Figure 2: Convex aggregate concrete mesostructure.

and PA_{i+1}, formed by the new point and the longest side, are longer than the minimum limit length $l_{\min}$, which is designed to ensure not to affect the division precision of the element, as expressed in the following equation:

$$l_{\min} = 0.2R \cdot \sin\left(\frac{\pi}{2(n-1)}\right). \tag{5}$$

Also, taking the efficiency of the extension into consideration, the growth of the newly formed polygon should be greater than the minimum $S_{\min}$, as in the following form:

$$S_{\min} = 0.3(S_A - S_B), \tag{6}$$

where S_A and S_B are the area of polygons before and after the new point is inserted, respectively.

Furthermore, the question is whether polygons can be achieved the requirement of convex polygons. According to the work in [40], the area criterion has been widely used to discriminate the convexity of polygon.

P (two conditions of the positions in point P are shown in Figures 5(a) and 5(b)) is a point in the plane, and its coordinate is (x, y). Besides, the area S_i of the triangle PA_iA_{i+1} can be calculated easily by the following equation:

$$S_i = \frac{1}{2}\begin{vmatrix} x & y & 1 \\ x_i & y_i & 1 \\ x_{i+1} & y_{i+1} & 1 \end{vmatrix}. \tag{7}$$

It is to be noted that when point P is inside the polygon, $S_i > 0$ $(i = 1, 2, \ldots, n)$; when point P is on the polygon boundary, at least $S_i = 0$ $(i = 1, 2, \ldots, n)$; when point P is outside the polygon, at least $S_i < 0$ $(i = 1, 2, \ldots, n)$. Besides, the internal area of the polygon $A_1A_2A_3 \cdots A_i \cdots A_n$ is Ω. In a word, the definition of point P is the inner point of the convex polygon that satisfies the following equations:

$$P \in \Omega, \quad S_i > 0, \tag{8}$$

$$P \in \Gamma, \quad \text{at least } S_i = 0, \tag{9}$$

$$P \notin \Omega, \quad \text{at least } S_i < 0. \tag{10}$$

For these three concisions, the area of polygon S should be the sum of area of every new formed polygon; that is,

$$S = S_1 + S_2 + S_3 + \cdots + S_{i-1} + S_i + S_{i+1} + S_{i+2} + \cdots + S_n. \tag{11}$$

As mentioned above, point P is a newly inserted vertex on the outside of the edge A_iA_{i+1}, which formed two triangles $PA_{i-1}A_i$ and $PA_{i+1}A_{i+2}$ with adjacent sides $A_{i-1}A_i$ and $A_{i+1}A_{i+2}$, respectively, shown in Figure 6. According to the area criterion when both the areas of the two triangles mentioned in equation (7) are positive, the newly formed is the convex polygon.

In addition, to prevent the occurrence of the aggregates invasion in Figure 7, the insertion point P should be checked. For the two cases of with different aggregate invasion, the point P can be inserted according to equations (7) and (10). The similar work was done in [18].

When the new insertion point meets all the above criteria, the insertion point is confirmed. And the extension ends until the area of generated polygonal is larger than the corresponding circle. Figure 8 presents the flowchart for the extension of the polygon-based framework.

4. Simulation Procedure

It has been known that the random aggregate model can simulate the internal structure of concrete. The heterogeneity of mesostructure will affect the mechanical properties of the material. To simulate more accurately, the random aggregate model was thus adopted. Besides, concrete is treated as a three-phase composite material consisting of aggregates, cement mortar, and the interfacial transition zones (ITZs) between the former two phases in the present model.

4.1. Mesoscale Model of Concrete. According to the experimental work, the particle size of fine aggregates is less than 5 mm which is uniformly distributed in the mortar matrix as part of the mortar phase. Namely, the mortar matrix is viewed as the homogenous phase in mesoscopic structure simplified for the purpose of convenience.

A typical "take-and-place" method was used to ensure that the coarse aggregates are placed randomly in the concrete specimen, which is similar with the work in [43]. Also, the coarse aggregates with large size assumed to be circle are divided into four levels ranging from 5 mm to 20 mm. Based on Fuller's grading curve, a simplified formula derived by Walraven J. C. is applied to calculate the amount of aggregate particles with different sizes in the two-dimensional plane. Moreover, as mentioned above, the circle aggregates are converted into convex aggregates. It should be noted that the take process and place process are conducted at the same time. Hence, newly generated aggregates are placed immediately one by one into the concrete specimen assuring that there is no overlapping with aggregates placed before and other components [18].

The divided regular triangular finite element mesh is projected directly onto the random aggregate model of concrete, as shown in Figure 9. It is found that dividing the size of the mesh element less than 1/4 of minimum aggregate

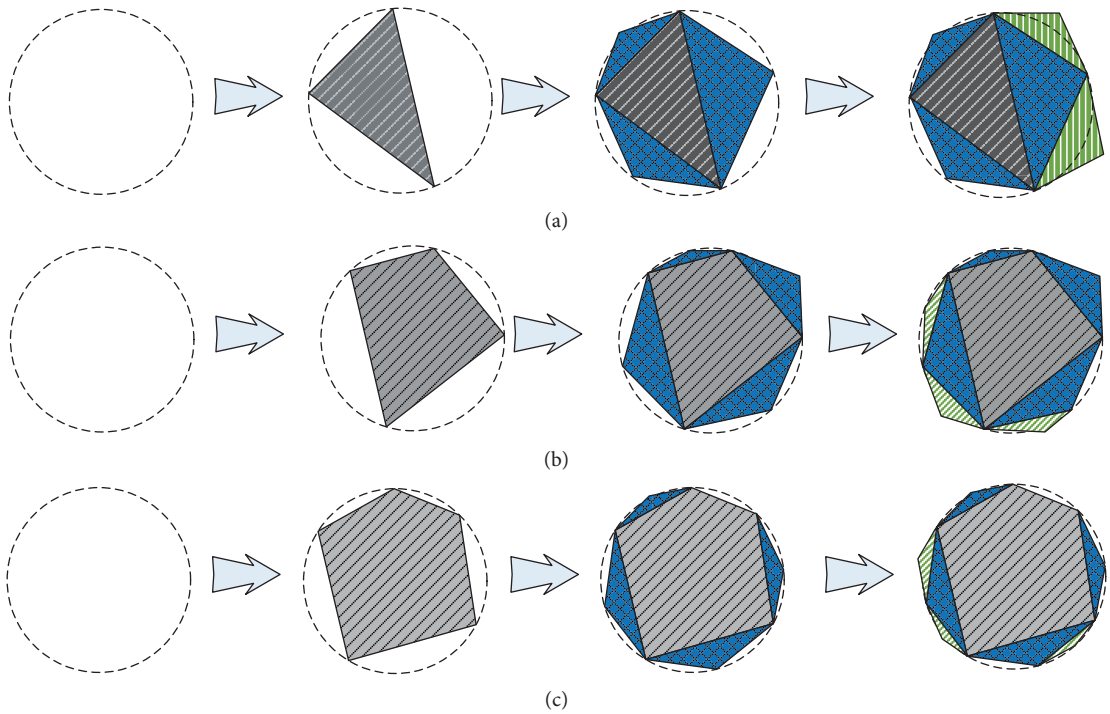

Figure 3: Convex polygon aggregate generation pattern.

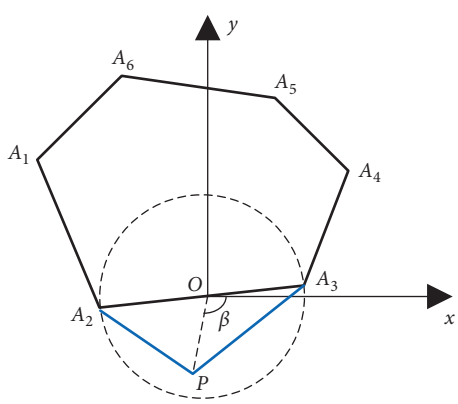

Figure 4: Generation of new vertices.

particle size would make the macroscopic mechanical properties of concrete more stable [44]. Accordingly, choose the mesh size of 1 mm considering that the particle size of the minimum aggregate is 5 mm in this model.

The element type is determined by the position of the element node, and the processes are as follows. When all the nodes of an element are in the area of coarse aggregate, it attributes to coarse aggregate. When all the nodes of an element are in the zone of cement mortar, it belongs to cement mortar. When some nodes of an element fall on the aggregate and some of the nodes are in the cement mortar, the element is judged as ITZ. At mesostructure, as depicted in Figure 9, blue, gray, and green regions denote aggregate, cement mortar, and ITZ, respectively. Then, according to the various types of

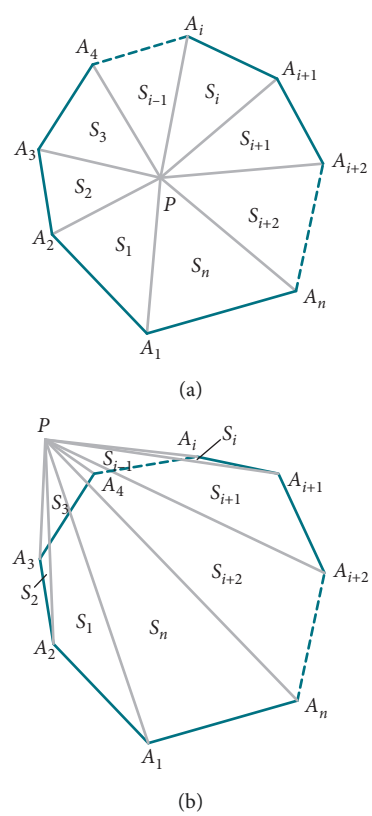

Figure 5: Convex polygon. (a) Point P on the polygon; (b) point P outside the polygon.

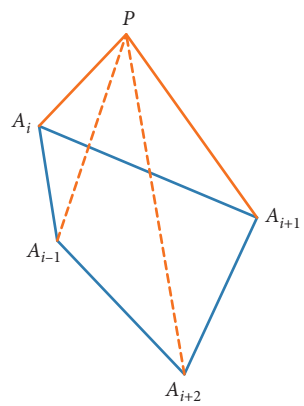

Figure 6: Convexity discrimination.

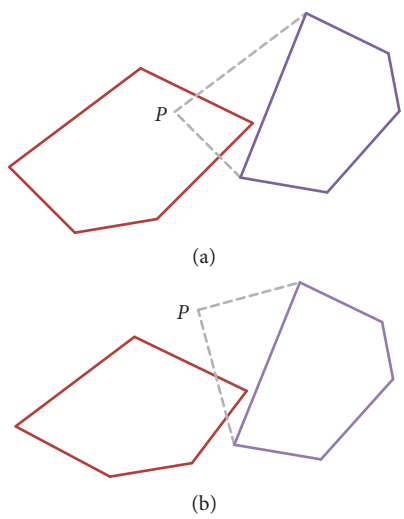

Figure 7: Aggregate invasion case. (a) Point P on the aggregate. (b) Point P outside the aggregate.

elements, the corresponding elements mechanical attributes are assigned.

To discover and analyze the fracture process and failure mechanism of concrete material subject to uniaxial compression, the load test with a square sample sized by 150 mm × 150 mm as shown in Figure 9 was simulated. In the test, the center at the bottom of the specimen overlaps with the center of the pressure plate with the testing machine, and the load is applied uniformly, as illustrated in Figure 10. Using the two-dimensional computation model of Figure 9 for simplicity and computational efficiency, the bottom surface boundary is fixed in the y-axis and the intermediate point is constrained in the x and y directions to prevent movements of the rigid body; besides the left, right, and top edges of the model are free in all directions. Additionally, in this study, without taking the end friction of the experimental device into account, displacements are applied to the stage loading as the step of 0.0045 mm/s in the y direction at the top boundary of the model. Furthermore, in the present calculation model, the maximum principal stress criterion is adopted.

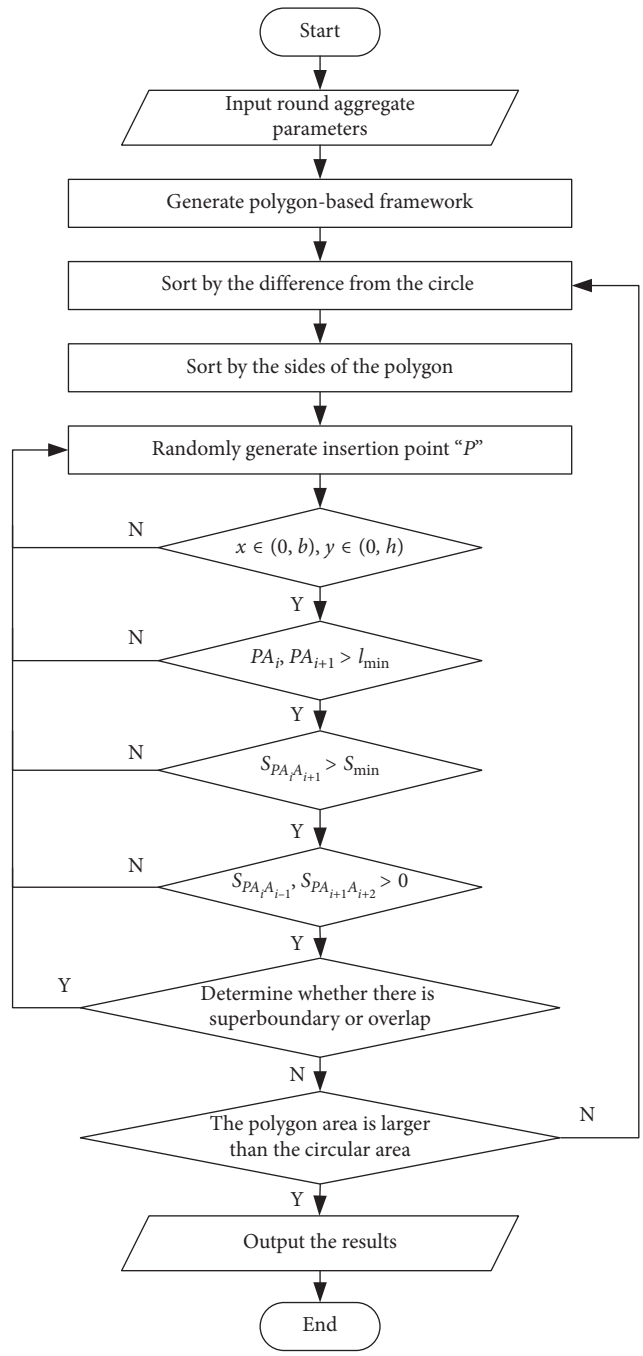

Figure 8: Convex extended subroutine flowchart.

4.2. Damage Constitutive. Because of the inhomogeneity of concrete internal structure, after subjected to the static loads, the damage and fracture processes within concrete are more complicated. With the characteristics of quasi-brittleness, the nonlinear behavior of concrete stress-strain full curve in the macroscopic structure is caused by the existence and development of microdefects, which is named as damage evolution in the mesoscale. It was found that the elastic damage mechanics model can effectively describe the mechanical properties of concrete composite [23–25]. Hence, mechanical properties of each component in concrete are assumed to be elastic damage in the present model. The

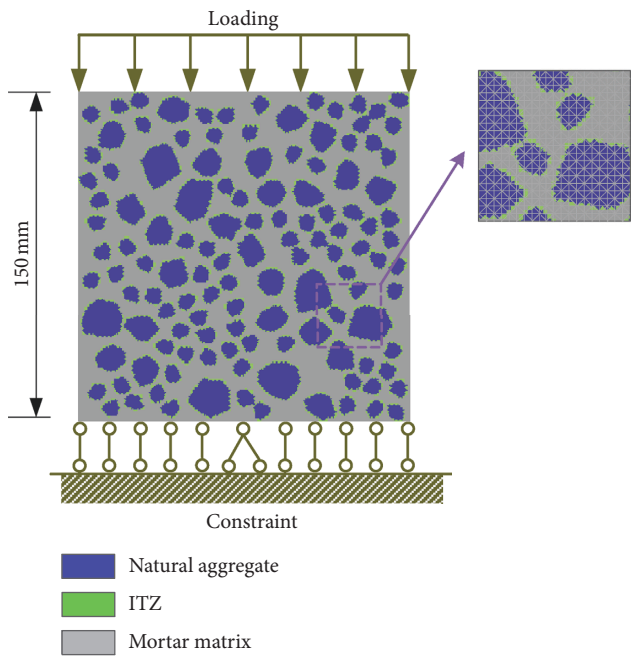

Figure 9: Simplified random aggregate loading model.

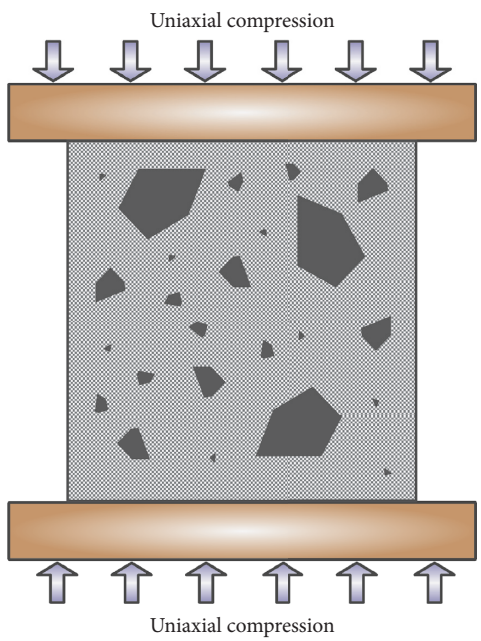

Figure 10: Compressive loading model.

phenomenon of stiffness degeneration is the macroscopic performance for the reason of nonlinear behavior of concrete. To predict the deformation and destruction of concrete structures, the damage factor is proposed to describe the state of material damage and mechanical effects.

For the constitutive relation behavior, aggregates, cement mortar, and ITZs are treated as isotropic material, while the material parameters are assigned to corresponding elements. In Figure 11, the softening behavior occurred until the peak strain corresponding to the compression strength is reached. The elastic damage constitutive relation of concrete

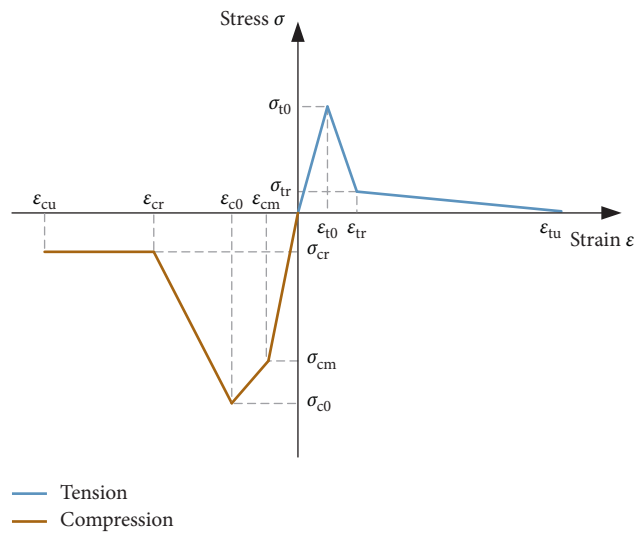

Figure 11: Nonlinear constitutive model for concrete.

can be easily obtained, according to Lemaitre strain equivalence principle [45], assuming that the deformation state of any damaged material can be expressed through the constitutive equation of the original nondestructive material depicted in Figure 12.

Therefore, the stress-strain relationship and effective elastic modulus of damage material can be written as

$$\begin{aligned} \sigma &= E\varepsilon, \\ E &= E_0(1-d), \end{aligned} \tag{12}$$

where σ and ε mean stress and strain of material, respectively, and E_0 and E are the elastic moduli of nondestructive and damaged material, respectively. The damage factor d is a constant, ranging from 0 to 1, according to the elastic damage constitutive model shown in Figure 11, compressive damage factor d_c and tensile damage factor d_t can be determined by equations (13) and (14), respectively. It can be noted from equations (13) and (14) that d is at the nondestructive state at 0 and d is completely destroyed at 1.

For compressive damage, a multistage linear damage constitutive model was proposed as follows:

$$d_c = \begin{cases} 0, & 0 < \varepsilon_c < \varepsilon_{c0}, \\ 1 - \dfrac{(1-\lambda(\varepsilon_{cr}/\varepsilon_c))(\alpha-\lambda)}{\alpha(1-\lambda)}, & \varepsilon_{c0} \le \varepsilon_c < \varepsilon_{cm}, \\ 1 - \dfrac{\lambda(\beta_c-1)\varepsilon_{c0}}{\alpha(\eta_c-1)\varepsilon_c} + \dfrac{\lambda(\beta_c-\eta_c)\varepsilon_{cr}}{\alpha(\eta_c-1)\varepsilon_c}, & \varepsilon_{cm} \le \varepsilon_c < \varepsilon_{cr}, \\ 1 - \dfrac{\lambda\beta_c\varepsilon_{cr}}{\alpha\varepsilon_c}, & \varepsilon_{cr} \le \varepsilon_c < \varepsilon_{cu}, \\ 1, & \varepsilon_{cu} \le \varepsilon_c, \end{cases} \tag{13}$$

where ε_{cm}, ε_{c0}, ε_{cr}, and ε_{cu} are yield compressive strain, peak compressive strain, residual compressive strain, and ultimate compressive strain, respectively, corresponding to

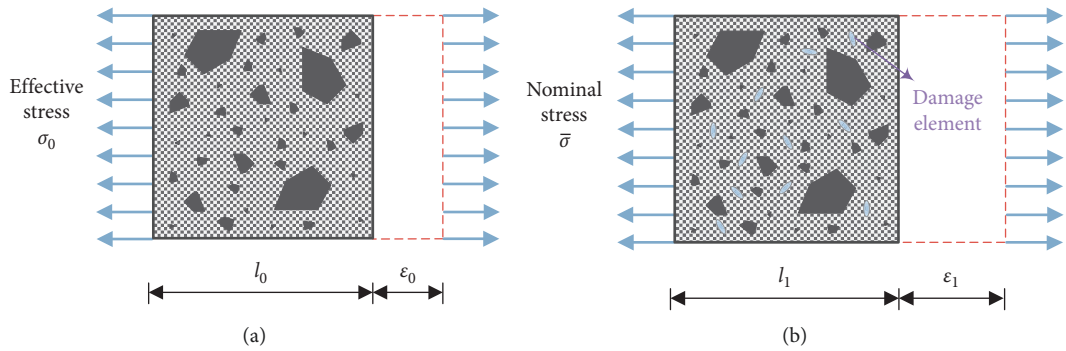

Figure 12: Lemaitre strain equivalence principle. (a) Before destruction. (b) After destruction.

$\varepsilon_{cm} = \lambda\varepsilon_{c0}$, $\varepsilon_{cr} = \eta_c\varepsilon_{c0}$, and $\varepsilon_{cu} = \xi_c\varepsilon_{c0}$. And yield compressive strain coefficient λ, residual compressive strain coefficient η_c, and ultimate compressive strain coefficient ξ_c of aggregates, cement mortar, and ITZs are listed in Table 1. Furthermore, in the value of the yield compressive stress coefficient $\alpha\,(\alpha = \sigma_{cm}/\sigma_{c0})$, residual and ultimate compressive stress coefficient $\beta_c\,(\beta_c = \sigma_{cr}/\sigma_{cu})$ depends on the different components as listed in Table 1.

For tensile damage,

$$d_t = \begin{cases} 0, & \varepsilon_t \le \varepsilon_{t0}, \\ 1 - \dfrac{\eta_t - \beta_t}{\eta_t - 1}\dfrac{\varepsilon_{t0}}{\varepsilon_t} + \dfrac{1-\beta_t}{\eta_t - 1}, & \varepsilon_{t0} \le \varepsilon_t < \varepsilon_{tr}, \\ 1 + \dfrac{\beta_t}{\eta_t - \xi_t}\left(1 + \xi_t\dfrac{\varepsilon_{t0}}{\varepsilon_t}\right), & \varepsilon_{tr} \le \varepsilon_t < \varepsilon_{tu}, \\ 1 & \varepsilon_{tu} \le \varepsilon_t, \end{cases} \tag{14}$$

where ε_{t0}, ε_{tr}, and ε_{tu} mean peak tensile strain, residual tensile strain, and ultimate tensile strain, respectively. The residual tensile strain coefficient is η_t $(\eta_t = \varepsilon_{tr}/\varepsilon_{t0})$ and ultimate tensile strain coefficient is δ_t $(\delta_t = \varepsilon_{tu}/\varepsilon_{t0})$ which are summarized in Table 1. In addition, the relation between peak tensile stress σ_{tr} and residual tensile stress σ_{t0} can be expressed as $\sigma_{tr} = \beta_t\sigma_{t0}$, where residual tensile stress coefficient β_t values vary with different components for concrete. Besides, ultimate tensile stress σ_{tu} is selected as zero herein the study.

Figure 11 plots the elastic damage constitutive relationship for mesoscopic composition of concrete. It can be noticed that the material properties (i.e., aggregates, cement mortar, and ITZs) are supposed to be linear until the peak stress is reached. Furthermore, the damage and deformation of the concrete material increase continuously with the increase of loading, while its stiffness, i.e., the elastic modulus decreased continuously, indicating the development of the softening phase. When the deformation reaches the residual strain, the concrete material is considered to be completely destroyed with stable bearing capacity.

4.3. Material Parameters and Weibull Distribution Model. For the three-phase medium, including aggregates, cement mortar, and ITZs, the parameters used initially in mesoscopic analysis models are summarized in Table 1, refer [40, 46–49]. It should be noted that the compressive strength and tensile strength of three media within concrete are available in Table 1.

Table 1: Material parameters of concrete mesostructure.

Materials	Cement mortar	Aggregate	ITZ
Elastic modulus (GPa)	20	53	15
Poisson's ratio	0.22	0.16	0.2
Tensile strength (MPa)	2.7	7	2.35
Compressive strength (MPa)	27	70	23.5
α	0.85	0.9	0.65
β_c	0.35	0.35	0.35
λ	0.25	0.8	0.25
η_c	8	10	6
ξ	20	20	20
β_t	0.3	0.3	0.3
η_t	5	6	4
ξ_t	20	20	20
m	6	15	3

As it is known that concrete is a material with randomness and discreteness, mechanical properties of its internal structure correspond to a certain distribution in statistical sense that can be handled with the probability method. In the past, numerous experimental researches [50–52] have indicated that the mechanical parameters of concrete obey the Weibull distribution, including elastic modulus and strength. According to the principle of the Weibull distribution, several attempts [53, 54] have been devoted to the study of fracture behavior for concrete. Therefore, in order to describe the heterogeneity of concrete materials more reasonably, the numerical simulation of this paper not only considers the random distribution of each phase material but also introduces the method of probability statistics. The mechanical properties of each microelement are assumed to satisfy the Weibull distribution function, considering the heterogeneity of constituent materials within concrete, and it can be defined as

$$f(u) = \frac{m}{u_0}\left(\frac{u}{u_0}\right)^{m-1}\exp\left[-\left(\frac{u}{u_0}\right)^m\right], \tag{15}$$

where u is the variable that satisfies this distribution and m means the uniformity of the material that determines the shape of the Weibull distribution density function. As listed in Table 1, the uniformity for three phases (i.e., aggregates,

cement mortar, and ITZs) of concrete was selected as 15, 6, and 3, respectively. The change can be found in Figure 13 that the intensity of elements tends to be uniform as the value of m increases. Besides, the parameter u_0 is related to the average value of the variable u.

5. Simulation Results and Analyses

The base force element method was extended on the previous work of [39] to model the damage process of the convex aggregate concrete by using the programming language FORTRAN in the numerical simulations.

In this study, the focus is on the investigation of fracture process and failure mechanism, and three specimens of concrete are established for the size of 150 mm × 150 mm. Figure 14 shows the comparison of the obtained experiment data of [55] (refer the work of Jin et al.) and simulation results. The good agreement illustrates that the base force element is able to apply to concrete modeling and has great feasibility and accuracy.

5.1. Failure Pattern. When subjected to external static loading, the crack position and failure pattern of concrete vary with the change of stress level, leading to an alteration of internal mechanical behavior for concrete [49]. Figure 15 demonstrates the whole fracture process from crack to destruction of concrete specimens under uniaxial compressive loading based on the present mesostructure method. What is more, the stress contour plots of two-dimensional concrete specimens are shown in Figure 16. In addition, the corresponding macroscopic failure relationship curve between stress and strain of concrete material is illustrated in Figure 14.

It can be seen from the stress contour plots in Figure 16 that the inhomogeneity of stress distribution, indicating the difference of mechanical properties between units, leads to the nonlinear behavior of concrete materials under external stress. In Figure 15, black means mesoscopic elements that achieve its compressive strength have entered the stage of failure under compressive loading. During the loading process, damage initially develops slowly with an elastic response at the low loading level. For the reason that aggregates are surrounded by mortar and ITZs, its strength does not work; in other words, the maximum principal stress in mortar is the largest (Figures 15 and 16). As the loading increases, the behavior of deformation accumulation and stress concentration causes the microcracks to appear at the ITZs, which is the weakest area in concrete with many microdefects. The damage to the specimens is getting faster, observing that the stress-strain curve shows a slightly convex curve in Figure 14. The damage is mainly in the area where the aggregate is concentrated. When the loading reaches the peak stress in Figure 14, the concrete specimen is almost totally in the damage stage. As the new damage zones constantly expand, destruction concentrates in the most damaged regions, resulting several local cracks. However, the cracks gradually extend into the mortar and go around when the aggregate particles with relatively high strength is

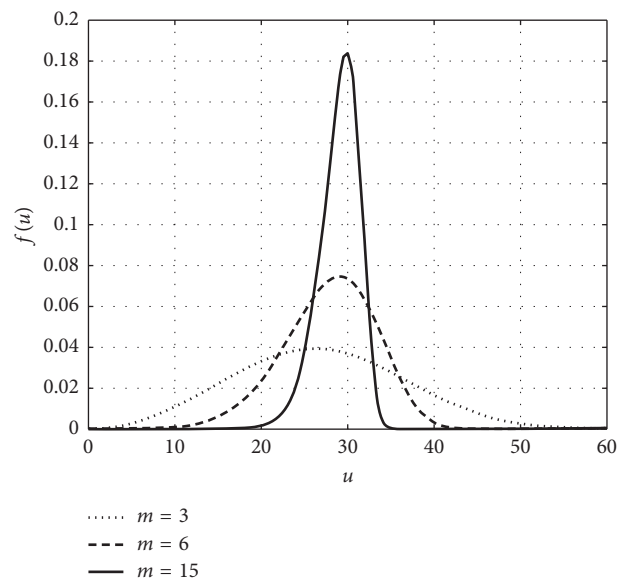

Figure 13: Probability density function for different degrees of homogeneity.

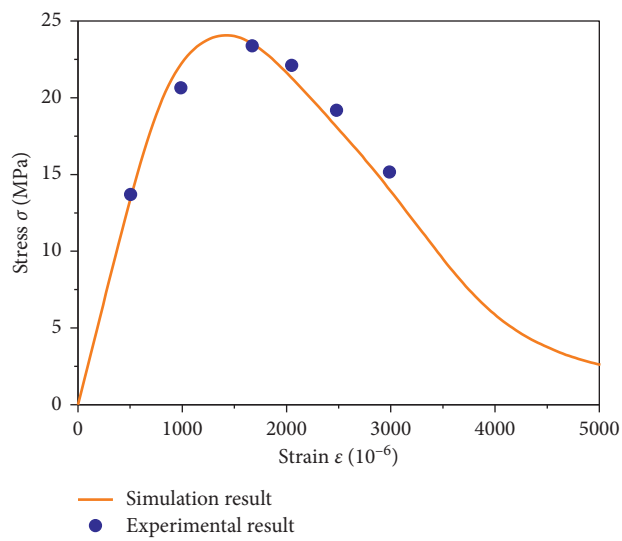

Figure 14: Comparison of macro-stress-strain curve between the numerical simulation and experimental result of Dilger et al. [55].

encountered until the cracks penetrate a section of the concrete specimen. Finally, more than one macroscopic cracks are formed that is parallel to the loading direction, causing the fracture damage of the concrete specimens and losing the bearing capacity, similar to the failure consequences of the test.

It can be observed from Figure 14 that initially the concrete internal material is stable, in which the whole specimen is mainly under elastic deformation state, and the stress-strain curve shows the characteristics of linear elasticity. Following this, the existence of microcracks reduced the effective sectional area of concrete; as a result, the stress continues to increase as strain increasing, while the elastic modulus decreases. After the stress peak strength, the concrete material enters the softening stage and the stress

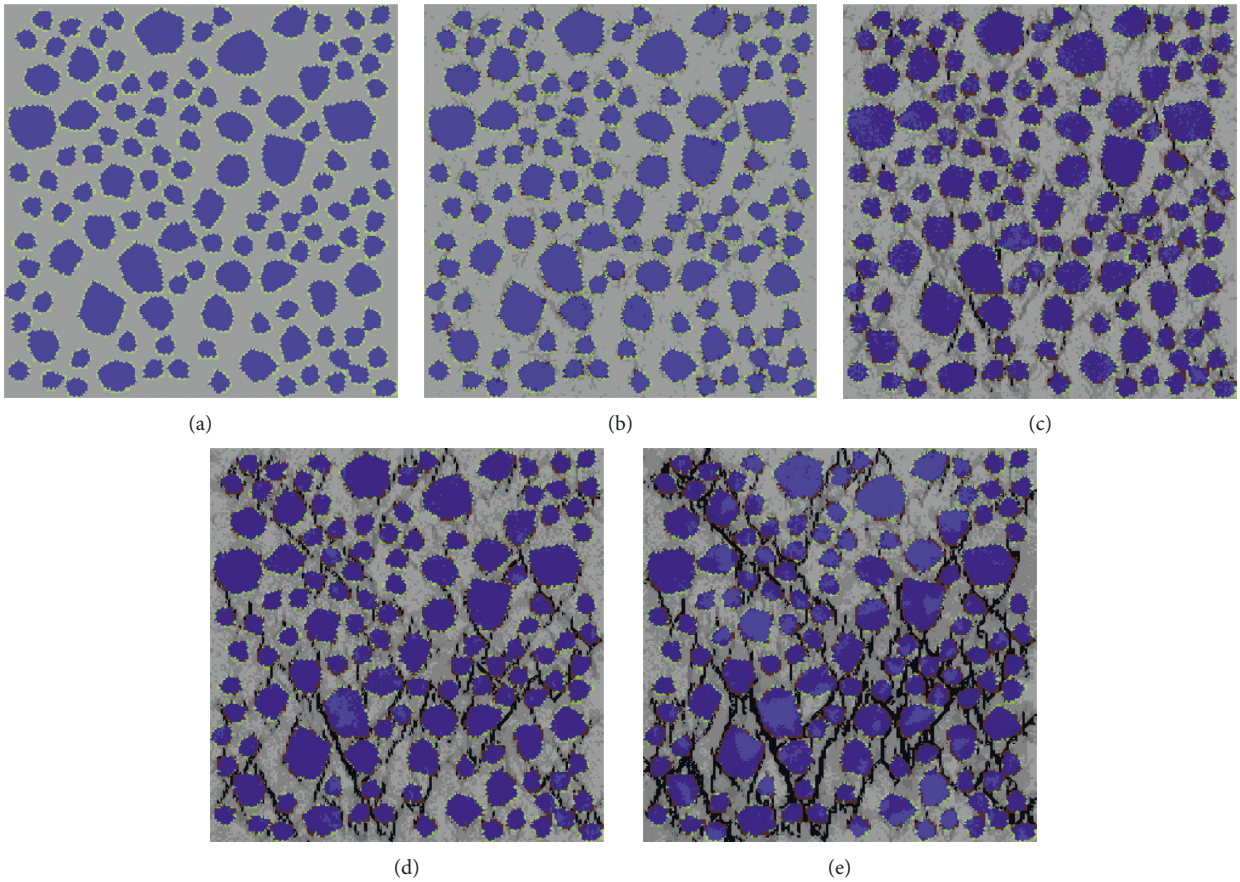

Figure 15: Failure process of concrete under uniaxial compression.

decreases with the increase of strain, presenting a nonlinear performance.

5.2. Effect of Aggregates Distribution. The difference in aggregate distribution will change the internal stress field under external loading. A group of the random aggregate model with three different aggregate distributions is established in the simulation as presented in Figure 17.

It can be observed that concrete with different aggregate distributions has distinct fracture paths in Figure 18. However, the corresponding stress-strain curve segment geometry overlaps in Figure 19, indicating that different aggregate distribution has little effect on the elastic modulus and strength of concrete in mesoscale. After the peak stress, the descending segments are significantly different mainly due to the damage process as shown in Figure 19.

5.3. Size Effect. The strength of concrete is measured by a cube specimen. As the size effect is widely recognized in the earlier efforts, it has practical significance to reveal the different size of concrete. A group of square concrete samples with the size of 100 mm × 100 mm, 150 mm × 150 mm, and 300 mm × 300 mm has been simulated in this study as showed in Figure 20.

Figure 21 shows the fracture damage of concrete specimens with different sizes, it can be found that the specimen size has slight effect on the failure pattern and fracture appears as tensile failure along the vertical direction.

Compared with the stress-strain curve presented in Figure 22 to study the influence of specimen size on strength, it can be noted that compressive peak strength of concrete decreases with the increase in the specimen size. Furthermore, the softening curve of the posterior peak segment is obviously different for varying sizes. The residual strength and ultimate strain decrease with the increase in the specimen size, indicating the brittleness of concrete specimen increases. This is because of the characteristics of nonhomogeneity in internal structure of concrete, including microcracks and microdefects. As the size of concrete specimen increases, the probability of defects increases and the dispersion of material performance increases. Concrete material is regarded with the characteristic of quasi-brittleness, and the damage is mainly caused by localization defects, which make the compressive strength reduction in the larger concrete specimen. And the results are consistent with the observation in [56].

5.4. Effect of Coarse Aggregate Content. As known, there is an optimum amount of coarse aggregate in concrete. In practical engineering, increasing the volume fraction of coarse aggregate can save the cost of concrete materials. Moreover, since the coarse aggregate has a higher strength than the other two mediums (i.e., cement mortar and ITZs),

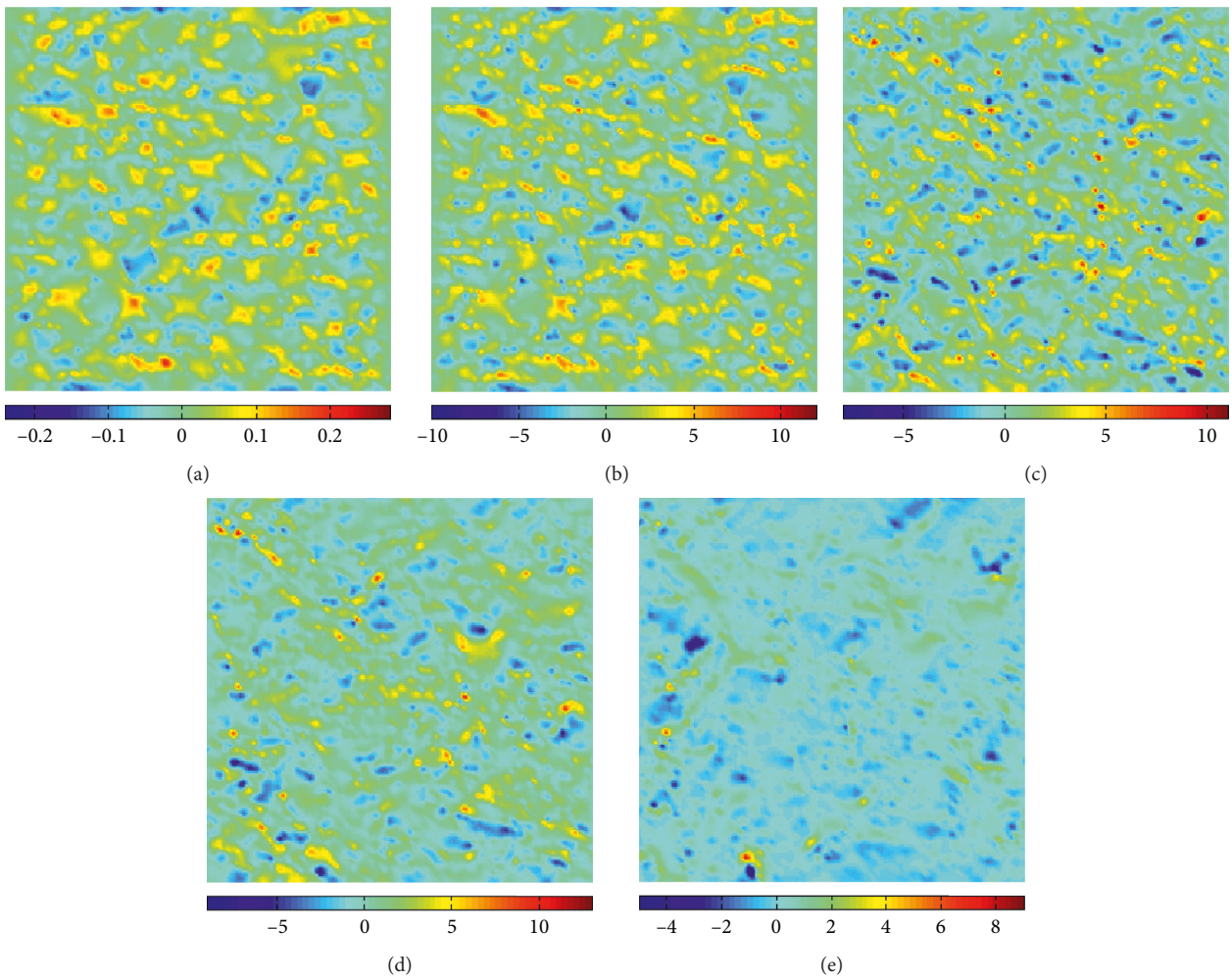

Figure 16: Failure process of the maximum principal stress contour plots under uniaxial compression.

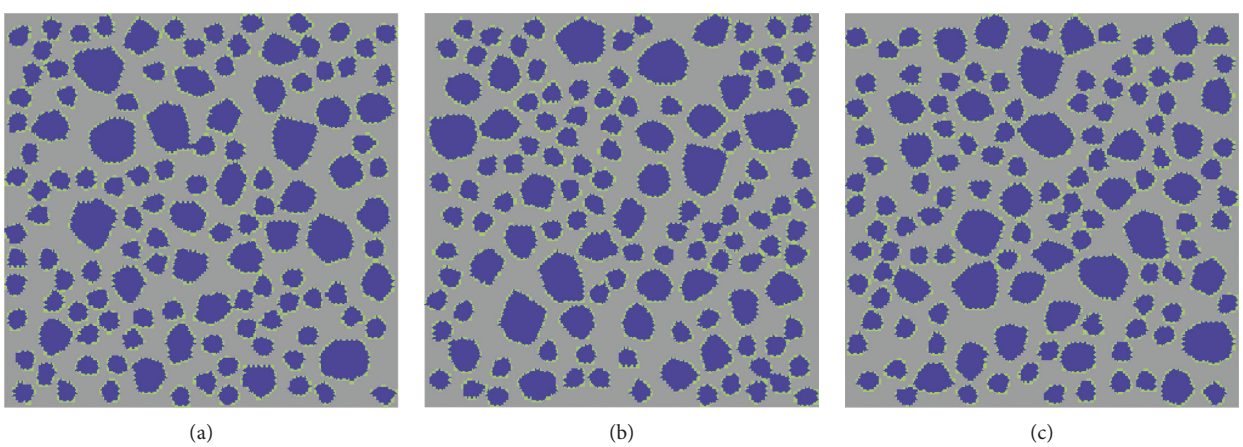

Figure 17: Random aggregate model of concrete with different aggregate distributions. (a) Specimen 1. (b) Specimen 2. (c) Specimen 3.

the strength of the concrete specimen increases with the increase of coarse aggregate volume fraction. However, too much coarse aggregate will reduce its adhesion to cement mortar, and correspondingly, the concrete integrity will deteriorate. To discover the effect of coarse aggregate content on the mechanical properties of concrete materials, the samples of concrete with seven different kinds of coarse aggregate content are employed. The volume fraction of coarse aggregate contains 25.61%, 27.92%, 30.27%, 32.60%, 34.93%, 37.25%, and 40.00% in the computations.

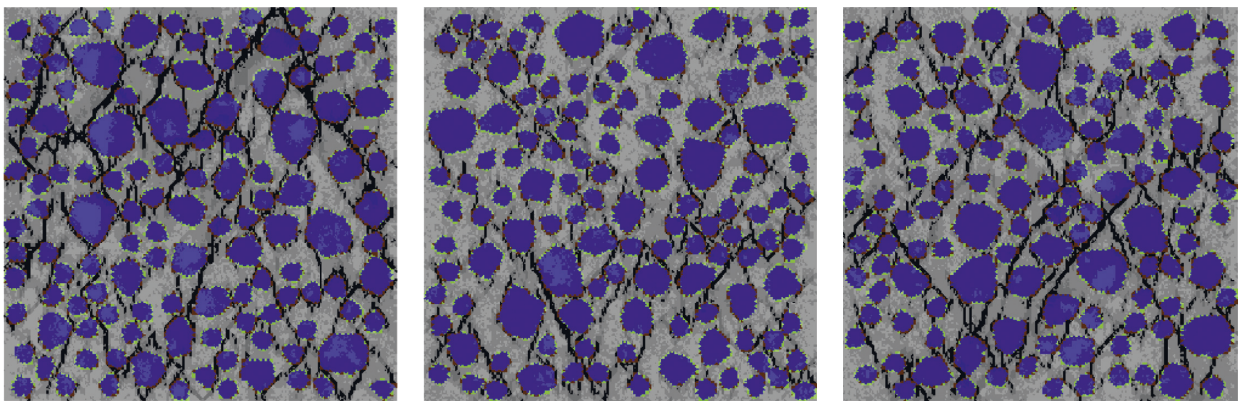

(a) (b) (c)

Figure 18: Uniaxial compressive damage process of concrete with different aggregate distributions. (a) Specimen 1. (b) Specimen 2. (c) Specimen 3.

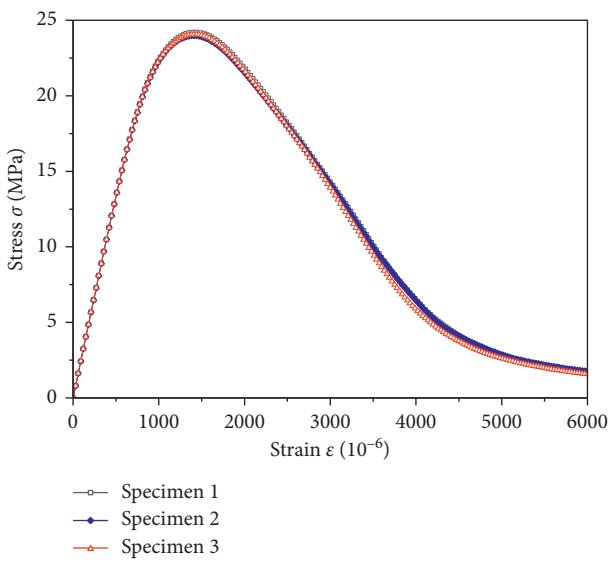

Figure 19: Macrocompressive stress-strain curve of concrete with different aggregate distributions.

Figure 23 plots the corresponding macroscopic compressive stress-strain curve for concrete specimens with different coarse aggregate volume fractions. It can be seen from Figures 23 and 24 that the elastic modulus of the initial elastic stage increases as the volume of coarse aggregate increases, indicating the stiffness of the concrete material increases. While with the increase of coarse aggregate content, the yield state is shorter and the peak strain decreases correspondingly. What is more, the peak stress is obviously improved, with the increasing coarse aggregate content; that is to say, the compressive strength of concrete specimen is improved. After the peak point, the bigger the volume content of coarse aggregate is, the faster the curve decreases, and the effect of softening will be obvious. Also one can know that the damage ductility of concrete specimen is better. To sum up, the impact of coarse aggregate content on mechanical properties of concrete specimens cannot be ignored.

5.5. Effect of End Friction. The constraint type has a great impact on the macroperformance of concrete which is determined by the boundary conditions of specimens. This is because that the change of end friction will take place for different boundary constraints. Therefore, to explore the end effect, two types of boundary conditions are utilized in the numerical simulation. As a comparison of the presented boundary condition, the bottom boundary of the concrete specimen is completely fixed in all the directions (i.e., x, y, and xy directions).

Figures 25 and 15, respectively, plot the damage pattern of nonfriction and friction (i.e., coefficient of friction $\mu = 1$ and $\mu = 0$) at the end of the concrete specimen. From the comparison of Figure 15, it can be noted that the end friction has a significant impact on the failure pattern of concrete material in uniaxial compression. In Figure 15, when $\mu = 0$, the crack first appears at the position of the loading end of the specimen. With the increase of loading, the cracks extend along the oblique direction from four corners at the end of the concrete specimen. The width of cracks after peak stress is wider, and the damage becomes more serious. Finally, the specimens lost its stability to be destroyed. This phenomenon is because that the friction at the end limits the transverse deformation of the two edges of the specimen while end limit is reduced in the middle of the specimen. A few oblique cracks are formed that is caused by maximum tensile stress. In one word, when the end friction exists, the concrete specimen is broken in the form of shear, and oblique cracks transfer from quadrangle to center, eventually resulting in a conical shape. As shown in Figure 25, for $\mu = 1$, it is mainly expressed as compressive failure forming the vertical cracks through the upper and lower surfaces in which the damage characteristic is obviously distinct from the boundary condition for end friction (i.e., $\mu = 0$).

The uniaxial compressive stress-strain curves for two types of end constraints are shown in Figure 26. One can find that for specimens of the same shape, the rising segment of the curve is almost identical. However, the softening slope after the peak of the stress-strain curve is steeper without considering the end friction. Also, it is found that the peak stress increases as the end friction increases. Generally

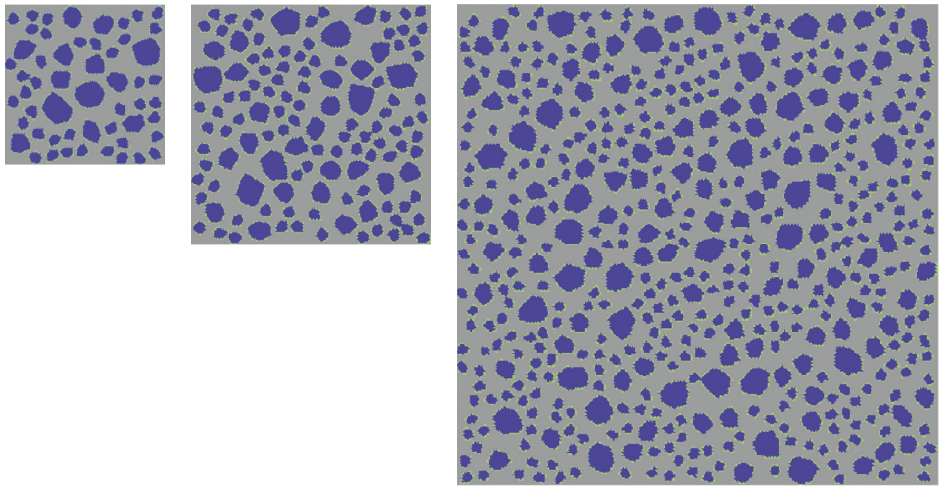

(a) (b) (c)

Figure 20: Random aggregate model of concrete for different sizes. (a) 100 mm. (b) 150 mm. (c) 300 mm.

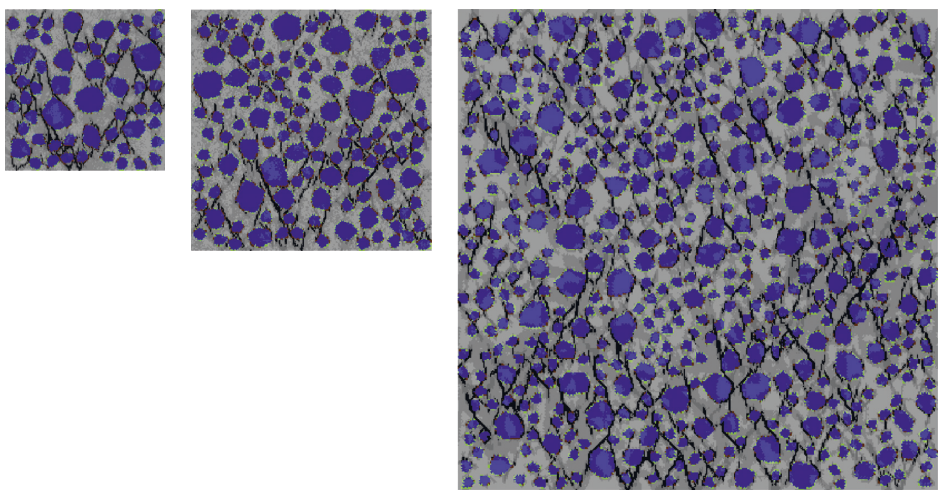

(a) (b) (c)

Figure 21: Failure patterns of concrete for different size models. (a) 100 mm. (b) 150 mm. (c) 300 mm.

speaking, end friction can effectively enhance the load-bearing capacity and improve the ductility capacity of concrete specimens.

6. Conclusions

The base force element method, a mesoscopic analysis method, is adopted for investigating the damage process and failure pattern of concrete subjected to uniaxial compression loading, taking the heterogeneity of its internal composition into account. In mesostructure, concrete is assumed to be a three-phase composite material including aggregate particles, cement mortar, and ITZs.

Based on the area criterion method, the aggregates within concrete are considered as convex polygon and a random aggregate model is established. Considering the nonlinear behavior of concrete after stress, an elastic damage constitutive relationship is employed in the model to describe the material parameters since the concrete material has the characteristics of heterogeneity and each medium owns its independent mechanical properties obeying the Weibull probability distribution. In comparison with the obtained test data, the feasibility of the numerical simulation method is confirmed. What is more, the detailed failure mechanism of concrete under uniaxial compression loading is analyzed. In addition, the influence of aggregates distribution, mesh sensitivity, prism specimen size, and end friction on strength and damage process is investigated. Some conclusions of this simulation results are obtained as follows:

(1) The numerical simulation results are in good agreement with the obtained experimental data which indicates the feasibility and accuracy of base force element method to model concrete in uniaxial compression.

(2) It is found that the multistage linear damage constitutive model proposed in this paper can better

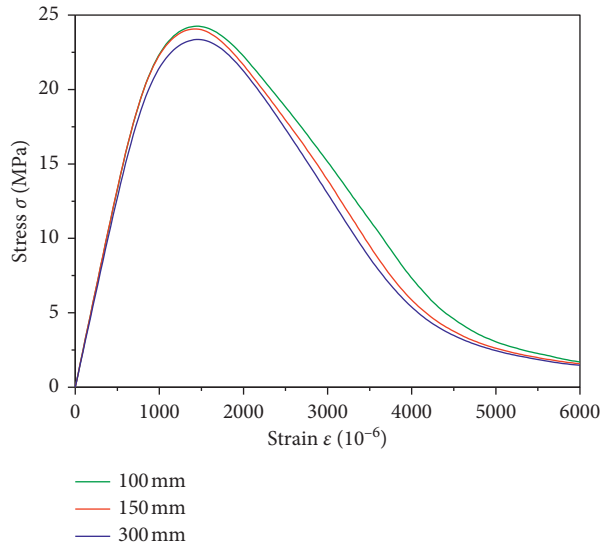

Figure 22: Macrocompressive stress-strain curve of concrete for different size models.

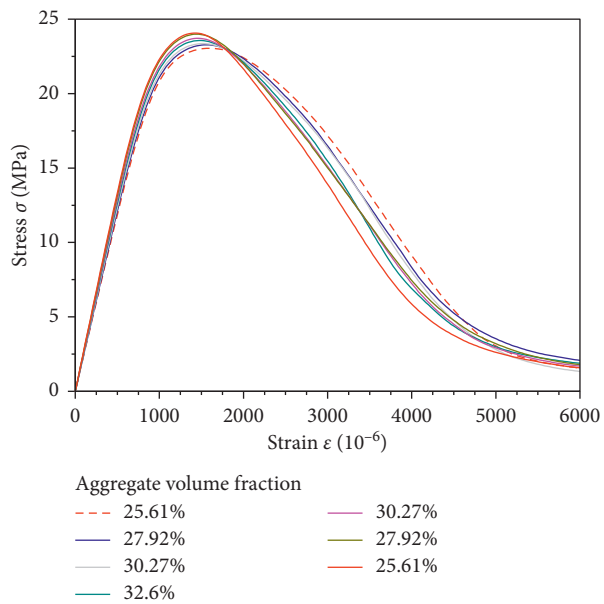

Figure 23: Macrocompressive stress-strain curve of the concrete specimen with different coarse aggregate contents.

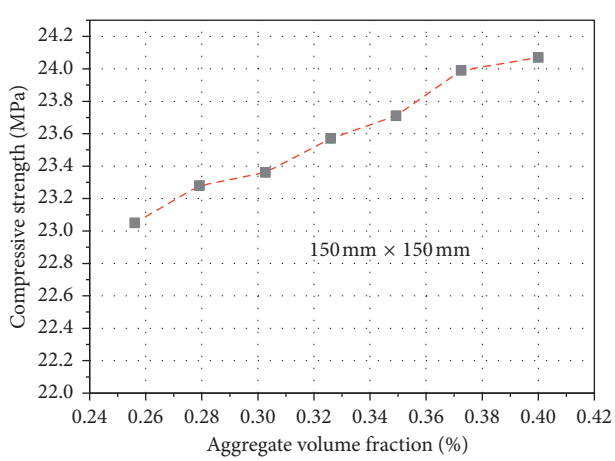

Figure 24: Comparison of compressive strength with different coarse aggregate contents.

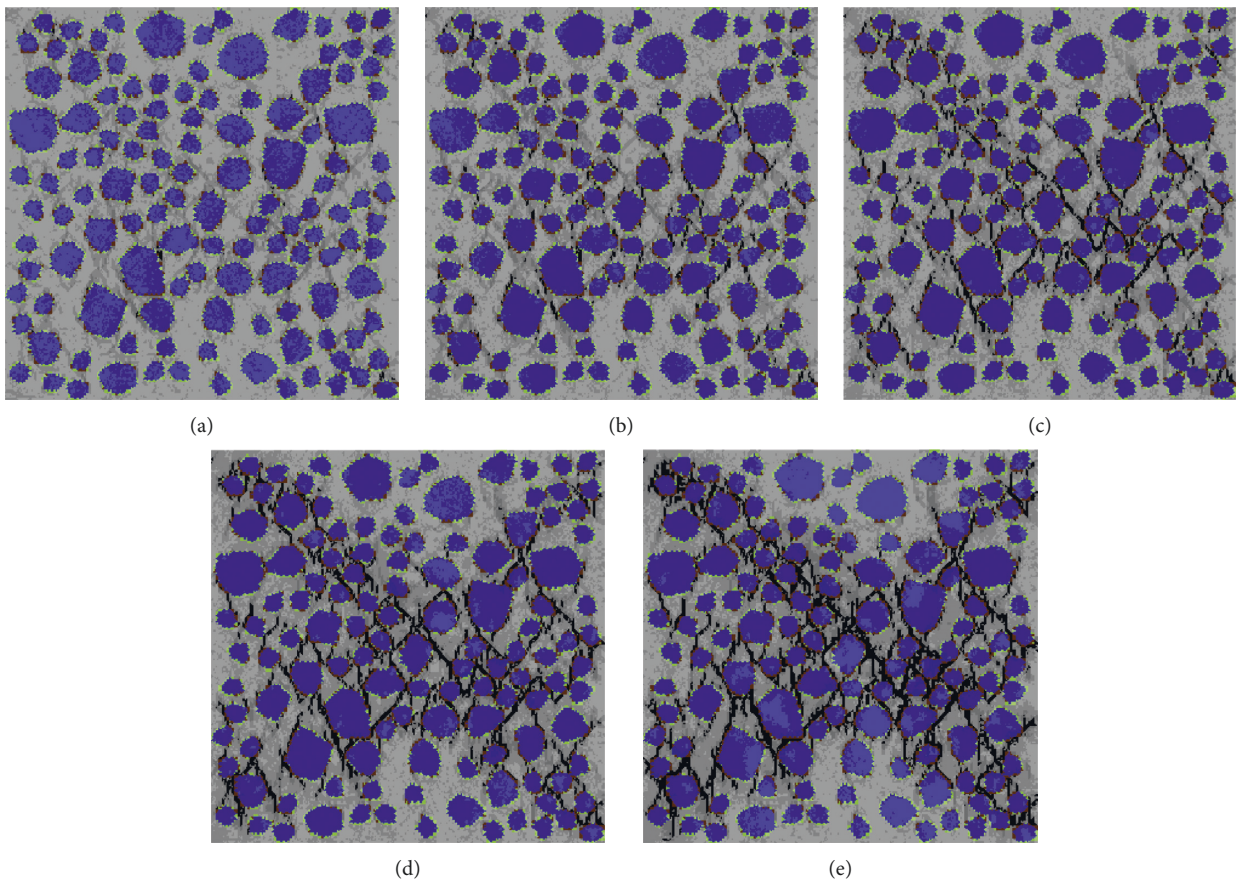

Figure 25: Failure patterns of concrete under different end friction constraints.

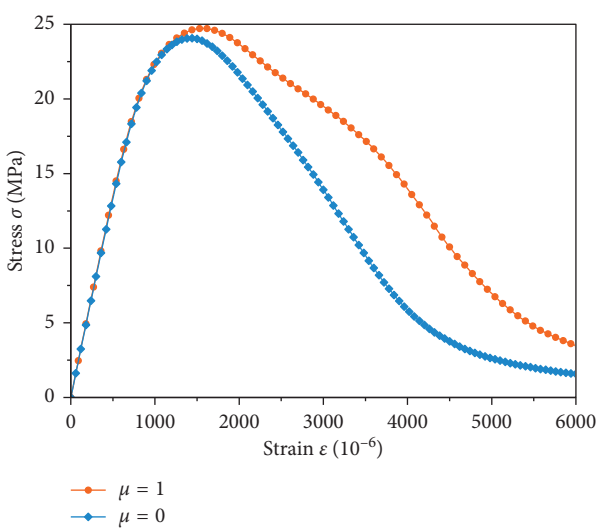

Figure 26: Comparison of the macroscopic stress-strain curve of concrete under different end friction constraints.

simulate the experiment than the linear elastic damage constitutive model.

(3) Numerical examples show that the convex polygonal aggregate can simulate the mesostructure of concrete well.

(4) The microcracks occur in the weakest zones as ITZs and then go around the aggregate and extend along the cement mortar forming several vertical cracks. Moreover, the failure pattern can be described as four stages, involving appearance of microcracks, propagation of cracks, the increasing of cracks, and fracture damage.

(5) Aggregate distribution form only has an effect on the generation of crack location and failure path; however, it does not affect the macroscopic elastic modulus and strength of concrete material.

(6) Size effect had significant effect on the macroscopic mechanical properties of the concrete material because the concrete material has the characteristics of the mesoscopic heterogeneity that larger size specimens have more internal defects after stress. Therefore, with the increase of the size of the concrete specimen, the uniaxial compressive strength decreases, while the brittleness of the concrete specimen becomes stronger after the damage.

(7) The uniaxial compressive strength of concrete specimens increased significantly with the increase of coarse aggregate content, but the brittleness of the softening segment is stronger. Therefore, it is of great practical significance to choose the content of coarse aggregate reasonably.

(8) The end friction can constrain the transverse deformation of the concrete specimen, which decreases with the increase of the distance from the end boundary. The end friction constraint causes the change of failure pattern for the concrete. Additionally, the existence of this effect can obviously improve the ductility capacity and uniaxial compression strength of the concrete square specimen.

Data Availability

The data used to support the findings of this study are included within the article.

Conflicts of Interest

The authors declare that there are no conflicts of interest regarding the publication of this paper.

Acknowledgments

This work was supported by the National Science Foundation of China (10972015 and 11172015), Beijing Natural Science Foundation (8162008), and Pre-Exploration Project of Key Laboratory of Urban Security and Disaster Engineering, Ministry of Education, Beijing University of Technology (USDE201404).

References

[1] F. H. Wittmann, P. E. Roelfstra, and H. Sadouki, "Simulation and analysis of composite structures," *Materials Science and Engineering*, vol. 68, no. 2, pp. 239–248, 1985.

[2] E. Schlangen and J. G. M. van Mier, "Simple lattice model for numerical simulation of fracture of concrete materials and structures," *Materials and Structures*, vol. 25, no. 9, pp. 534–542, 1992.

[3] C. Xu, L. Jin, Z. Ding, D. Li, and X. Du, "Size effect tests of high-strength RC columns under eccentric loading," *Engineering Structures*, vol. 126, pp. 78–91, 2016.

[4] E. Syroka-Korol, J. Tejchman, and Z. Mróz, "FE analysis of size effects in reinforced concrete beams without shear reinforcement based on stochastic elasto-plasticity with nonlocal softening," *Finite Elements in Analysis and Design*, vol. 88, no. 10, pp. 25–41, 2014.

[5] L. Jin, L. Dong, X. Du, and Z. Ding, "Experimental and numerical study on size effect in eccentrically loaded stocky RC columns," *Journal of Structural Engineering*, vol. 143, no. 2, article 04016170, 2016.

[6] Z. P. Bažant, "Size effect in blunt fracture: concrete, rock, metal," *Journal of Engineering Mechanics*, vol. 110, no. 4, pp. 518–535, 1984.

[7] K. Duan, X. Hu, and F. H. Wittmann, "Scaling of quasi-brittle fracture: boundary and size effect," *Mechanics of Materials*, vol. 38, no. 1-2, pp. 128–141, 2006.

[8] C. G. Hoover and Z. P. Bažant, "Cohesive crack, size effect, crack band and work-of-fracture models compared to comprehensive concrete fracture tests," *International Journal of Fracture*, vol. 187, no. 1, pp. 133–143, 2014.

[9] Z. P. Bažant and B. H. Oh, "Crack band theory for fracture of concrete," *Matériaux Et Construction*, vol. 16, no. 3, pp. 155–177, 1983.

[10] B. L. Karihaloo and P. Nallathambi, "Fracture toughness of plain concrete from three-point bend specimens," *Materials and Structures*, vol. 22, no. 3, pp. 185–193, 1989.

[11] S. Xu and X. Zhang, "Determination of fracture parameters for crack propagation in concrete using an energy approach," *Engineering Fracture Mechanics*, vol. 75, no. 15, pp. 4292–4308, 2008.

[12] M. F. Kaplan, "Crack propagation and the fracture of concrete," *American Concrete Institute Journal*, vol. 58, no. 5, pp. 591–610, 1961.

[13] Y. Jenq and S. P. Shah, "Two parameter fracture model for concrete," *Journal of Engineering Mechanics*, vol. 111, no. 10, pp. 1227–1241, 1985.

[14] A. Hillerborg, M. Modéer, and P.-E. Petersson, "Analysis of crack formation and crack growth in concrete by means of fracture mechanics and finite elements," *Cement and Concrete Research*, vol. 6, no. 6, pp. 773–781, 1976.

[15] Z. P. Bažant and Y. W. Kwon, "Failure of slender and stocky reinforced concrete columns: tests of size effect," *Materials and structures*, vol. 27, no. 2, pp. 79–90, 1994.

[16] J. Kozicki and J. Tejchman, "Effect of aggregate structure on fracture process in concrete using 2D lattice model," *Archives of Mechanics*, vol. 59, no. 4-5, pp. 365–384, 2007.

[17] A. R. Mohamed and W. Hansen, "Micromechanical modeling of crack-aggregate interaction in concrete materials," *Cement and Concrete Composites*, vol. 21, no. 5-6, pp. 349–359, 1999.

[18] Z. M. Wang, A. K. H. Kwan, and H. C. Chan, "Mesoscopic study of concrete I: generation of random aggregate structure and finite element mesh," *Computers & Structures*, vol. 70, no. 5, pp. 533–544, 1999.

[19] X. Du, L. Jin, and G. Ma, "Meso-element equivalent method for the simulation of macro mechanical properties of concrete," *International Journal of Damage Mechanics*, vol. 22, no. 5, pp. 617–642, 2012.

[20] J. P. B. Leite, V. Slowik, and J. Apel, "Computational model of mesoscopic structure of concrete for simulation of fracture processes," *Computers & Structures*, vol. 85, no. 17-18, pp. 1293–1303, 2007.

[21] H.-K. Man and J. G. M. van Mier, "Damage distribution and size effect in numerical concrete from lattice analyses," *Cement and Concrete Composites*, vol. 33, no. 9, pp. 867–880, 2011.

[22] J. Lemaitre and J. L. Chaboche, "Mécanique des matériaux solides," *Chamonix*, vol. 16, no. 4, pp. 273–279, 1985.

[23] K. E. Loland, "Continuous damage model for load-response estimation of concrete," *Cement and Concrete Research*, vol. 10, no. 3, pp. 395–402, 1980.

[24] D. Krajcinovic and G. U. Fonseka, "The continuous damage theory of brittle materials, Part 1: general theory," *Journal of Applied Mechanics*, vol. 48, no. 4, pp. 809–815, 1981.

[25] J. Mazars and G. Pijaudier-Cabot, "Continuum damage theory-application to concrete," *Journal of Engineering Mechanics*, vol. 115, no. 2, pp. 345–365, 1989.

[26] S. P. Shah and G. Winter, "Inelastic behavior and fracture of concrete," *ACI Journal Proceedings*, vol. 63, no. 9, pp. 925–930, 1966.

[27] O. Buyukozturk, "Stress-strain response and fracture of a concrete model in biaxial loading," *ACI Journal Proceedings*, vol. 68, no. 8, pp. 590–599, 1971.

[28] Z. P. Bazant, M. R. Tabbara, M. T. Kazemi, and G. Pijaudier-Cabot, "Random particle model for fracture of aggregate or fiber composites," *Journal of Engineering Mechanics*, vol. 116, no. 8, pp. 1686–1705, 1990.

[29] Q. Yu, J.-L. Le, C. G. Hoover, and Z. P. Bažant, "Problems with Hu-Duan boundary effect model and its comparison to size-shape effect law for quasi-brittle fracture," *Journal of Engineering Mechanics*, vol. 136, no. 1, pp. 40–50, 2010.

[30] C. G. Hoover and Z. P. Bažant, "Comparison of the Hu-Duan boundary effect model with the size-shape effect law for quasi-brittle fracture based on new comprehensive fracture tests," *Journal of Engineering Mechanics*, vol. 140, no. 3, pp. 480–486, 2014.

[31] X. Hu, J. Guan, Y. Wang, A. Keating, and S. Yang, "Comparison of boundary and size effect models based on new developments," *Engineering Fracture Mechanics*, vol. 175, no. 15, pp. 146–167, 2017.

[32] C. Zhang, X. Hu, Z. Wu, and Q. Li, "Influence of grain size on granite strength and toughness with reliability specified by normal distribution," *Theoretical and Applied Fracture Mechanics*, vol. 96, pp. 534–544, 2018.

[33] R. Al-Raoush and M. Alsaleh, "Simulation of random packing of polydisperse particles," *Powder Technology*, vol. 176, no. 1, pp. 47–55, 2007.

[34] H. Ma, W. Xu, and Y. Li, "Random aggregate model for mesoscopic structures and mechanical analysis of fully-graded concrete," *Computers & Structures*, vol. 177, pp. 103–113, 2016.

[35] P. L. Liu and K. G. Liu, "Selection of random field mesh in finite element reliability analysis," *Journal of Engineering Mechanics*, vol. 119, no. 4, pp. 667–680, 1993.

[36] G. D. Schutter and L. Taerwe, "Random particle model for concrete based on delaunay triangulation," *Materials and Structures*, vol. 26, no. 2, pp. 67–73, 1993.

[37] Y. Peng and Y. Liu, "Base force element method of complementary energy principle for large rotation problems," *Acta Mechanica Sinica*, vol. 25, no. 4, pp. 507–515, 2009.

[38] Y. C. Gao, "A new description of the stress state at a point with applications," *Archive of Applied Mechanics*, vol. 73, no. 3-4, pp. 171–183, 2003.

[39] Y. Peng, Y. Liu, J. Pu, and L. Zhang, "Application of base force element method to mesomechanics analysis for recycled aggregate concrete," *Mathematical Problems in Engineering*, vol. 2013, Article ID 292801, 8 pages, 2013.

[40] Y. C. Li, H. F. Ma, H. Q. Chen, and X. Hu, "Approach to generation of random convex polyhedral aggregate model and plotting for concrete meso-mechanics," *Journal of Hydraulic Engineering*, vol. 37, no. 5, pp. 588–592, 2006.

[41] M. Choinska, A. Khelidj, G. Chatzigeorgiou, and G. Pijaudier-Cabot, "Effects and interactions of temperature and stress-level related damage on permeability of concrete," *Cement and Concrete Research*, vol. 37, no. 1, pp. 79–88, 2007.

[42] L. Jin, R. Zhang, X. Du, and Y. Li, "Multi-scale analytical theory of the diffusivity of concrete subjected to mechanical stress," *Construction and Building Materials*, vol. 95, pp. 71–185, 2015.

[43] P. Wriggers and S. O. Moftah, "Mesoscale models for concrete: homogenisation and damage behaviour," *Finite Elements in Analysis and Design*, vol. 42, no. 7, pp. 623–636, 2006.

[44] L.-P. Guo, A. Carpinteri, R. Roncella, A. Spagnoli, W. Sun, and S. Vantadori, "Fatigue damage of high performance concrete through a 2D mesoscopic lattice model," *Computational Materials Science*, vol. 44, no. 4, pp. 1098–1106, 2009.

[45] J. Lemaitre, J. L. Chaboche, and A. K. Maji, "Mechanics of solid materials," *Journal of Engineering Mechanics*, vol. 119, no. 3, pp. 642-643, 1993.

[46] K. R. Wu and X. Zhang, *Building Materials*, Tongji University Press, Shanghai, China, 1994, in Chinese.

[47] J. A. Wang, J. Lubliner, and P. J. M. Monteiro, "Effect of ice formation on the elastic moduli of cement paste and mortar," *Cement and Concrete Research*, vol. 18, no. 6, pp. 874–885, 1988.

[48] M. P. Lutz, P. J. M. Monteiro, and R. W. Zimmerman, "Inhomogeneous interfacial transition zone model for the bulk modulus of mortar," *Cement and Concrete Research*, vol. 27, no. 7, pp. 1113–1122, 1997.

[49] A. K. H. Kwan, Z. M. Wang, and H. C. Chan, "Mesoscopic study of concrete II: nonlinear finite element analysis," *Computers & Structures*, vol. 70, no. 5, pp. 545–556, 1999.

[50] K. Trustrum and A. D. S. Jayatilaka, "On estimating the weibull modulus for a brittle material," *Journal of Materials Science*, vol. 14, no. 5, pp. 1080–1084, 1979.

[51] Y. Lei, N. P. O'Dowd, E. P. Busso, and G. A. Webster, "Weibull stress solutions for 2-D cracks in elastic and elastic-plastic materials," *International Journal of Fracture*, vol. 89, no. 3, pp. 245–268, 1998.

[52] J. G. M. van Mier, M. R. A. van Vliet, and K. W. Tai, "Fracture mechanisms in particle composites: statistical aspects in lattice type analysis," *Mechanics of Materials*, vol. 34, no. 11, pp. 705–724, 2002.

[53] X. X. He and Z. H. Xie, "Experimental study on statistical parameters of concrete strength based on weibull probability distribution," *Key Engineering Materials*, vol. 477, pp. 224–232, 2011.

[54] B. R. Kim and H. K. Lee, "Elastic-damage modeling for particulate composites considering cumulative damage," *International Journal of Damage Mechanics*, vol. 20, no. 1, pp. 131–158, 2010.

[55] W. H. Dilger, R. Koch, and R. Kowalczyk, "Ductility of plain and confined concrete under different strain rates," *Journal of the American Concrete Institute*, vol. 81, no. 1, pp. 73–81, 1984.

[56] C. Liu, B. Wu, Y. Yang, and J. R. Martí-Vargas, "Discussion: size effect on compressive behaviours of normal-strength concrete cubes made from demolished concrete blocks and fresh concrete," *Magazine of Concrete Research*, vol. 67, no. 8, pp. 430–432, 2013.